
This copy is for your personal, non-commercial use only.

If you wish to distribute this article to others, you can order high-quality copies for your colleagues, clients, or customers by [clicking here](#).

Permission to republish or repurpose articles or portions of articles can be obtained by following the guidelines [here](#).

The following resources related to this article are available online at www.sciencemag.org (this information is current as of May 4, 2014):

Updated information and services, including high-resolution figures, can be found in the online version of this article at:

<http://www.sciencemag.org/content/344/6183/523.full.html>

Supporting Online Material can be found at:

<http://www.sciencemag.org/content/suppl/2014/04/16/science.1250368.DC1.html>

A list of selected additional articles on the Science Web sites **related to this article** can be found at:

<http://www.sciencemag.org/content/344/6183/523.full.html#related>

This article **cites 42 articles**, 7 of which can be accessed free:

<http://www.sciencemag.org/content/344/6183/523.full.html#ref-list-1>

This article appears in the following **subject collections**:

Genetics

<http://www.sciencemag.org/cgi/collection/genetics>

We went on to examine whether cis-eQTLs shared across cell types have similar direction and effect sizes. The comparison of the effect size for an eQTL (most significant SNP per gene) in the two cell types (Fig. 2C) showed concordance in effect size for most eQTLs (Pearson's $r = 0.79$). However, in 42 genes, the most significant SNP was associated with discordant directional effects across cell types: The allele associated with higher expression in one cell type is associated with lower expression in the other (Fig. 2D and fig. S14). We identified another dimension of cell type specificity: 6% of genes with cis-eQTLs shared across cell types are influenced by different, independent SNPs in each of the two cell types. Furthermore, 7% of independent SNPs in T cells and 11% in monocytes were associated with expression levels of more than one gene, with several SNPs affecting different genes in a cell type-dependent manner (Fig. 2E).

Leveraging 6341 SNPs (LD-pruned to $r^2 < 0.4$) associated with one or more of 415 human diseases or traits [National Institutes of Health genome-wide association study (GWAS) catalog] (14), we note 887 independent SNPs that influence expression of 1088 genes in cis (tables S16 and S17). To distinguish coincidental colocalizations of GWAS and eQTL associations, we used regulatory trait concordance (RTC) scores (15), which assesses whether a cis-eQTL and a trait association are tagging the same functional variant. Applying a stringent RTC threshold of 0.9, we identified 106 GWAS SNPs in T cells for which the trait and expression associations may be tagging the same effect; in monocytes, 123 GWAS SNPs met this criterion. Given the cell types profiled in our study, we found the expected significant enrichment (permutation $P < 1 \times 10^{-4}$) for cis-eQTLs among autoimmune disease-associated variants: Of the 425 GWAS SNPs associated with one or more autoimmune disease, 143 have cis-regulatory effects on 164 genes in monocytes and/or T cells (fig. S15 and tables S18 and S19).

Disease and trait-associated cis-eQTLs show more cell type specificity than average cis-eQTLs. Using BMA-HM, we find that 46% of all trait-associated variants are monocyte-specific, 29% are T cell-specific, and 25% are shared (Fig. 3A). In addition, variants associated with some diseases display a preponderance of T cell-specific cis-regulatory effects: These include susceptibility alleles for multiple sclerosis, rheumatoid arthritis, and type 1 diabetes (Fig. 3, A and B). On the other hand, Alzheimer's disease (AD), Parkinson's disease (PD), lipid traits, and type 2 diabetes susceptibility alleles are enriched in monocyte-specific effects (Fig. 3, A and B). In fact, the AD susceptibility alleles are significant eQTLs only in monocytes (Fig. 3B and figs. S16 and S17). Because the targeted genes are mostly expressed in both monocytes and T cells, this observed polarization is not driven by the lack of expression of the implicated genes in T cells (fig. S18).

On the basis of these results, we suggest that the inflammatory component of susceptibility to neurodegenerative diseases may be more strongly driven by the myeloid compartment of the immune system. This is consistent with the altered phagocytic function that we have reported in monocytes of individuals carrying the *CD33* AD susceptibility variant (16). The putative role of inflammation has previously been invoked in aging-related neurodegenerative diseases such as AD and PD (17), but our results bring a genetic underpinning and candidate pathways to these observations. Because our study examines young and healthy individuals, we provide support for a role of myeloid cells in the prodromal phase of neurodegenerative diseases. Functionally, we cannot say that blood-derived monocytes themselves are the key cell type; they are likely to be proxies for the infiltrating macrophages (which differentiate from monocytes) and/or resident microglia found at the sites of neuropathology. Both of these cell types share many of the transcriptome patterns of monocytes.

Despite its inherent logistic challenges, the profiling of purified primary cells from multiple human populations was clearly beneficial in several respects, including the reduction of the credible set of variants associated with a given trait. Though the majority of eQTLs are shared, the ImmVar study provides clear examples of context specificity of eQTLs and has yielded insights into the relative role of two representative cell types in exerting the functional consequences of disease-associated variants. Further, the depletion of disease-associated eQTLs with effects in both cell types is intriguing and suggests that the evolutionary history of cell-specific and pleiotropic variants is an important area of future investigation. Overall, this component of the ImmVar Project represents

a strong foundation for future explorations of the role of disease susceptibility variants in an increasingly diverse matrix of cell types, stimuli, and in vivo contexts.

References and Notes

1. B. E. Stranger *et al.*, *PLoS Genet.* **8**, e1002639 (2012).
2. T. Lappalainen *et al.*, *Nature* **501**, 506–511 (2013).
3. A. Battle *et al.*, *Genome Res.* **24**, 14–24 (2014).
4. B. P. Fairfax *et al.*, *Nat. Genet.* **44**, 502–510 (2012).
5. H. J. Westra *et al.*, *Nat. Genet.* **45**, 1238–1243 (2013).
6. D. L. Nicolae *et al.*, *PLoS Genet.* **6**, e1000888 (2010).
7. G. Trynka *et al.*, *Nat. Genet.* **45**, 124–130 (2013).
8. M. T. Maurano *et al.*, *Science* **337**, 1190–1195 (2012).
9. G. R. Abecasis *et al.*, *Nature* **491**, 56–65 (2012).
10. T. Flutre, X. Wen, J. Pritchard, M. Stephens, *PLoS Genet.* **9**, e1003486 (2013).
11. J. D. Storey, R. Tibshirani, *Proc. Natl. Acad. Sci. U.S.A.* **100**, 9440–9445 (2003).
12. B. Han, E. Eskin, *Am. J. Hum. Genet.* **88**, 586–598 (2011).
13. B. E. Bernstein *et al.*, *Nature* **489**, 57–74 (2012).
14. L. A. Hindorf *et al.*, *Proc. Natl. Acad. Sci. U.S.A.* **106**, 9362–9367 (2009).
15. A. C. Nica *et al.*, *PLoS Genet.* **6**, e1000895 (2010).
16. E. M. Bradshaw *et al.*, *Nat. Neurosci.* **16**, 848–850 (2013).
17. C. K. Glass, K. Saijo, B. Winner, M. C. Marchetto, F. H. Gage, *Cell* **140**, 918–934 (2010).

Acknowledgments: We thank the study participants in the Phenogenetic Project for their contributions. We are grateful to T. Flutre and X. Wen for assistance with running the Bayesian model averaging software. This work was supported by U.S. National Institute of General Medical Sciences grant RC2 GM093080 (C.B.). T.R. is supported by the NIH F32 Fellowship (F32 AG043267). Gene expression data are deposited in the National Center for Biotechnology Information Gene Expression Omnibus under accession no. GSE56035.

Supplementary Materials

www.sciencemag.org/content/344/6183/519/suppl/DC1
Materials and Methods
Figs. S1 to S25
Tables S1 to S19
References (18–31)

11 December 2013; accepted 8 April 2014
10.1126/science.1249547

Reconstructing the DNA Methylation Maps of the Neandertal and the Denisovan

David Gokhman,¹ Eitan Lavi,¹ Kay Prüfer,² Mario F. Fraga,³ José A. Riancho,⁴ Janet Kelso,² Svante Pääbo,² Eran Meshorer,^{1,5*} Liran Carmel^{1*}

Ancient DNA sequencing has recently provided high-coverage archaic human genomes. However, the evolution of epigenetic regulation along the human lineage remains largely unexplored. We reconstructed the full DNA methylation maps of the Neandertal and the Denisovan by harnessing the natural degradation processes of methylated and unmethylated cytosines. Comparing these ancient methylation maps to those of present-day humans, we identified ~2000 differentially methylated regions (DMRs). Particularly, we found substantial methylation changes in the *HOXD* cluster that may explain anatomical differences between archaic and present-day humans. Additionally, we found that DMRs are significantly more likely to be associated with diseases. This study provides insight into the epigenetic landscape of our closest evolutionary relatives and opens a window to explore the epigenomes of extinct species.

The high-coverage genomes of the Denisovan (1) and the Neandertal (2), from whom present-day humans split 550,000 to 765,000 years ago (2), allowed the comparison of our

DNA to that of our closest extinct relatives. However, differences could be sought exclusively at the sequence level and consequently did not provide direct insights regarding epigenetic

regulation, which likely underlies many of the traits that distinguish these human groups.

DNA methylation is a key hallmark of gene activity in mammals, where it occurs almost exclusively in cytosines in the context of CpG dinucleotides. In promoters, it is inversely correlated with expression level, and in intergenic regions it is linked to the activity of enhancers and insulators and to silencing transposable elements (3, 4).

Classic methods to measure full methylomes are impracticable to apply to archaic samples because of damage to the ancient DNA. However, the natural process of cytosine deamination, in

which unmethylated cytosines decay with time to uracils and methylated cytosines decay to thymines (5), has been shown to carry information regarding general trends of genome methylation (5, 6). Sequencing protocols of ancient DNA trim uracils but leave thymines unprocessed (5). Therefore, positions in which cytosines were methylated pre-mortem are expected to have a higher fraction of reads with thymines compared with unmethylated positions. Consequently, the fraction of CpG→TpG substitutions (hereinafter, C→T ratio) may serve as a proxy for the levels of methylation in ancient DNA (Fig. 1A and fig. S1).

We computed, for every CpG in the human genome, a C→T ratio in each of the archaic human genomes. Positions that were expected to represent true pre-mortem thymines rather than postmortem deamination were excluded (7). We then compared the Neandertal and Denisovan C→T ratios to experimentally measured methylation in bone (osteoblast) cells of a present-day human (8). The samples were obtained from the femur, costae, and tibia bones of a young female and therefore highly resemble the Neandertal and Denisovan samples [obtained from limb bones of young females (1, 2)]. For both ancient genomes, the correlation between binned present-day meth-

ylation and archaic C→T ratios was ~0.98 (7) (Fig. 1B).

In order for deamination to serve as a reliable proxy for DNA methylation, it should display a stochastic behavior that is homogenous along the genome. By using the genome of a ~4000-year-old Eskimo, the sequencing protocol of which provides a direct measure for deamination rates (9), we show that every region in the genome has the same probability to undergo deamination (7). Such homogeneity is expected given the fast post-mortem degradation of cellular structure and proteins that are therefore unlikely to bias deamination across tens of thousands of years.

In order to account for the stochastic nature of deamination, we computed for each CpG a mean C→T ratio by using a sliding window over neighboring CpGs (7) (fig. S2 and table S1). The correlation between the C→T ratio and present-day human methylation is apparent also when examining specific genomic regions (Fig. 2A and fig. S3A). Furthermore, our method is highly robust not only to coverage variation, which could potentially bias C→T ratio through reduced coverage in uracil-trimmed regions, but also to potential differences in deamination rate between methylated and unmethylated cytosines (7) (fig. S4).

¹Department of Genetics, Alexander Silberman Institute of Life Sciences, Hebrew University of Jerusalem, Jerusalem 91904, Israel. ²Department of Evolutionary Genetics, Max Planck Institute for Evolutionary Anthropology, D-04103 Leipzig, Germany. ³Cancer Epigenetics Laboratory, University Institute of Oncology of Asturias–Cajastur Social Program (IUOPA), University of Oviedo, Oviedo and Centro Nacional de Biotecnología–Consejo Superior de Investigaciones Científicas, Madrid, Spain. ⁴Department of Medicine, Hospital Universitario Marqués de Valdecilla, University of Cantabria, Instituto de Investigación Marqués de Valdecilla, Santander, Spain. ⁵Edmond and Lily Safra Center for Brain Sciences, Hebrew University of Jerusalem, Jerusalem 91904, Israel.
*Corresponding author. E-mail: liran.carmel@huji.ac.il (L.C.); meshorer@huji.ac.il (E.M.)

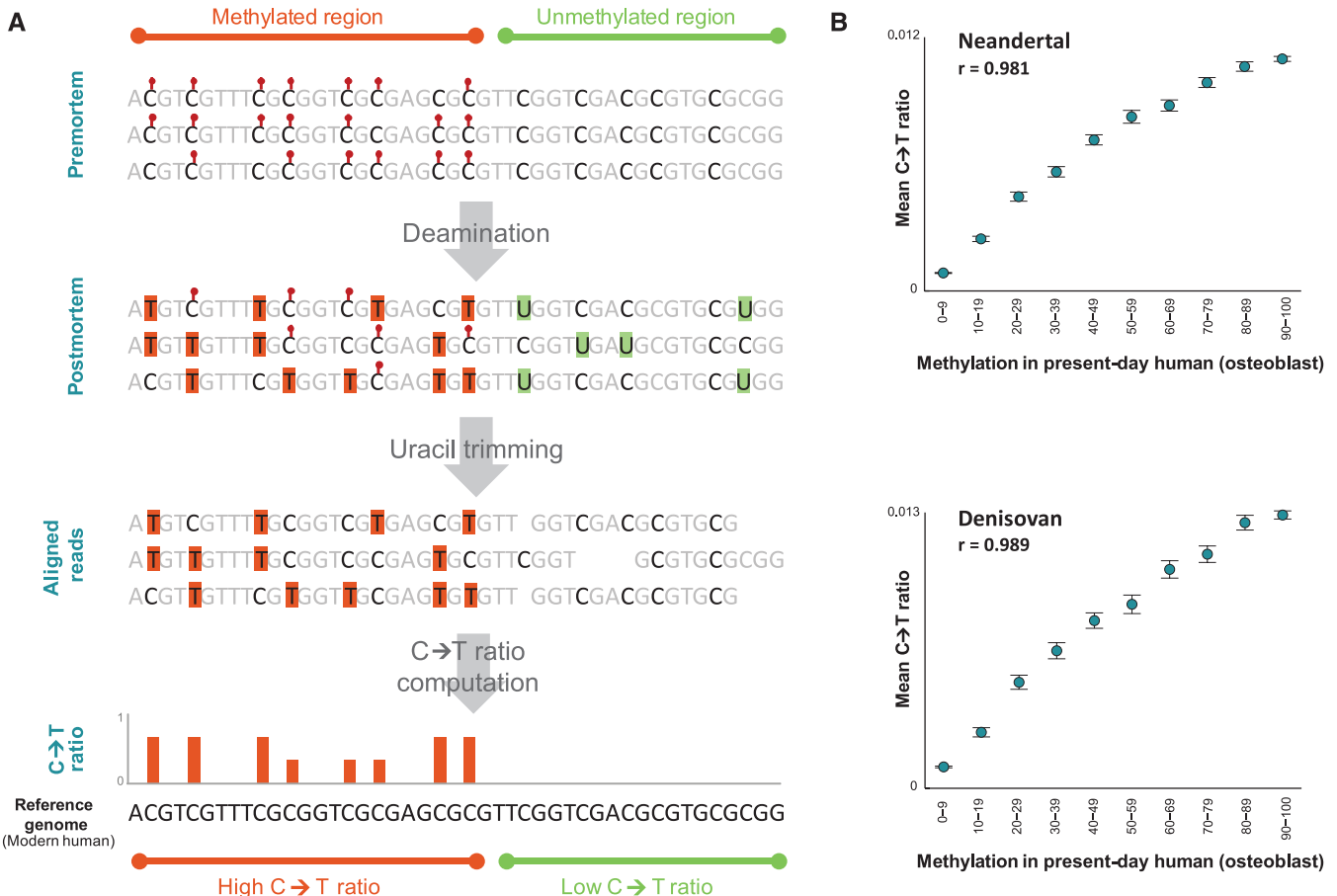


Fig. 1. C→T ratio is a proxy for ancient DNA methylation. (A) Scheme of the processes that enable the reconstruction of ancient methylation by using C→T ratios. **(B)** C→T ratios in archaic humans are highly correlated with

measured methylation in present-day humans. CpGs were binned according to their measured methylation level in human osteoblast cells, and for each bin a mean C→T ratio was computed. Error bars represent one standard deviation.

We then scaled the C→T ratios to represent premortem methylation percentages (7). The reconstructed archaic methylation in single CpGs shows strong correlation to measured present-day methylation ($r = 0.77$ in the Denisovan; $r = 0.79$ in the Neandertal) (Fig. 2B). Next, we investigated CpG islands, which tend to be hypomethylated in mammalian genomes (3). The reconstructed methylation in CpG islands falls within the range of values in present-day humans (fig. S3B). We also investigated 3804 housekeeping genes (10), whose promoters are constitutively hypomethylated (4). The reconstructed methylation shows strong hypomethylation and falls within the range of 16 present-day human tissues taken from 20 individuals (11) (Fig. 3A and fig. S3C). Taken together, these results suggest that the C→T ratio can be used as a proxy for premortem methylation and that genome-wide methylation maps can be reconstructed after tens of thousands of years.

As expected from groups that diverged recently, over 99% of both archaic genomes show no significant methylation differences compared to the present-day human. However, in each archaic human we found ~1100 differentially methylated regions (DMRs) (7). We divided the DMRs

according to where the methylation change has likely occurred, that is, into Neandertal-specific, Denisovan-specific, and present-day human-specific DMRs. DMRs that could not be confidently assigned to a specific lineage were tagged as unclassified DMRs (7) (Fig. 3B and table S2). Because housekeeping genes serve fundamental functions in all cells, we expected them to present low rates of methylation changes. Reassuringly, despite constituting ~10% of genes, none of the housekeeping genes harbors DMRs ($P = 1.7 \times 10^{-36}$, hypergeometric test). Last, when comparing differences in methylation to differences in sequence, we observed a significant overlap between the two, as expected if some of the methylation changes were driven by sequence changes ($P < 10^{-6}$, randomization test).

A difference in methylation between an archaic and a present-day human does not necessarily imply a fixed difference between the human groups. This difference can stem from variability within a population or from the comparison of close, yet not identical, cell types (osteoblasts versus whole bones). Hence, we compared the archaic methylation to 37 bones samples taken from osteoblasts and whole bones (12–14). We sought reliable DMRs, in which the archaic methylation significantly differs from that in modern

bones. These samples were measured with 27K arrays and provided information for ~5% of DMRs. In most DMRs, archaic methylation was significantly different from the 37 bones and therefore classified as reliable [false discovery rate (FDR) < 0.01 , z-test] (tables S2 and S3).

DMRs for which data from bones was not available were compared with 25 samples of 23 tissues from 20 individuals representing both sexes, different ethnicities, and ages ranging from 6 to 88 (8). Over 50% of DMRs had stable methylation levels across modern samples, but were significantly different in the archaic humans, and are thus likely to represent reliable DMRs (7) ($FDR < 0.01$ (tables S2 and S3)).

A key regulator of limb development is the 5' HOXD cluster (15), which includes five genes (*HOXD9* to *HOXD13*). We identified three DMRs within the HOXD locus (Fig. 4) and two intergenic DMRs located 20- and 25-kb upstream to the cluster in a putative enhancer region (16) (table S2). In both archaic humans, we detected hypermethylation in the *HOXD9* promoter and in the *HOXD10* gene body, whereas in present-day humans these regions are hypomethylated in all 37 bone samples (methylation = $5 \pm 2\%$;

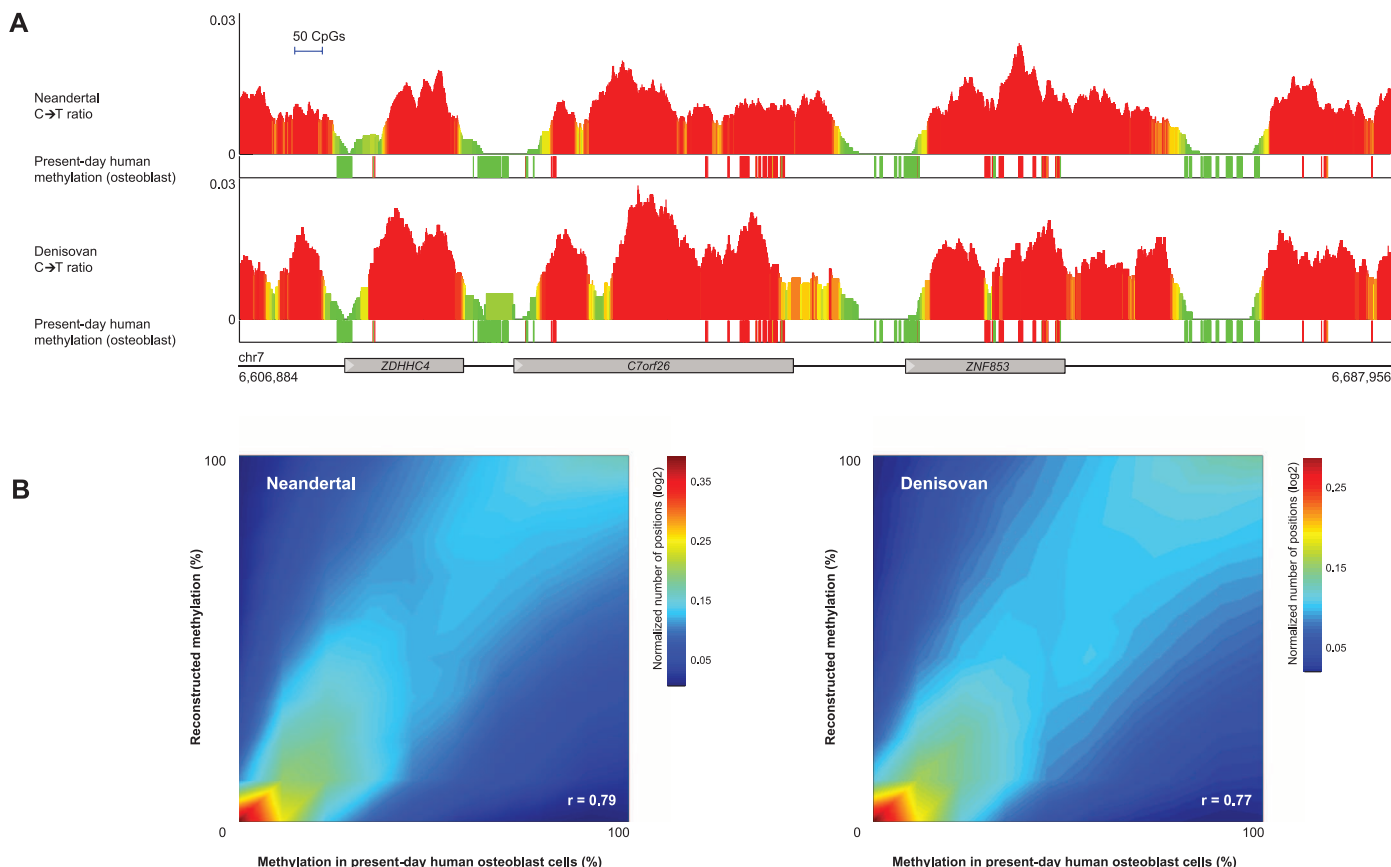


Fig. 2. Reconstructed archaic methylation relative to present-day human methylation. (A) An exemplary region (chromosome 7, 6,606,884 to 6,687,956) demonstrating that reconstructed archaic methylation patterns follow present-day human patterns. C→T ratio and measured methylation are color-coded with a gradient from green (unmethylated) to red (methylated). The bottom line shows genes in the region. For visual clarity, osteoblast

methylation in present-day humans appears twice, below each of the C→T ratio lanes. (B) Normalized heat maps of present-day human methylation versus archaic reconstructed methylation for all single CpG positions across the genome. The hot region along the diagonal line shows that, in most CpG positions, reconstructed methylation matches measured present-day methylation.

$FDR < 1.7 \times 10^{-30}$, z-test). In addition, we found the gene body of *HOXD9* to be hypermethylated in the Denisovan (Fig. 4 and table S2). These DMRs imply linked regulation of *HOXD9* and

HOXD10, consistent with observations in mouse (17). Distinctions between present-day and Neandertal limbs include larger femur articulations (18), robust hands and fingers (19), broader el-

bow and knee joints (18, 20), more-curved radius and femur (18, 20), and shorter limbs (18, 20). All of these features were shown in mouse and human to result from changes in the HOXD

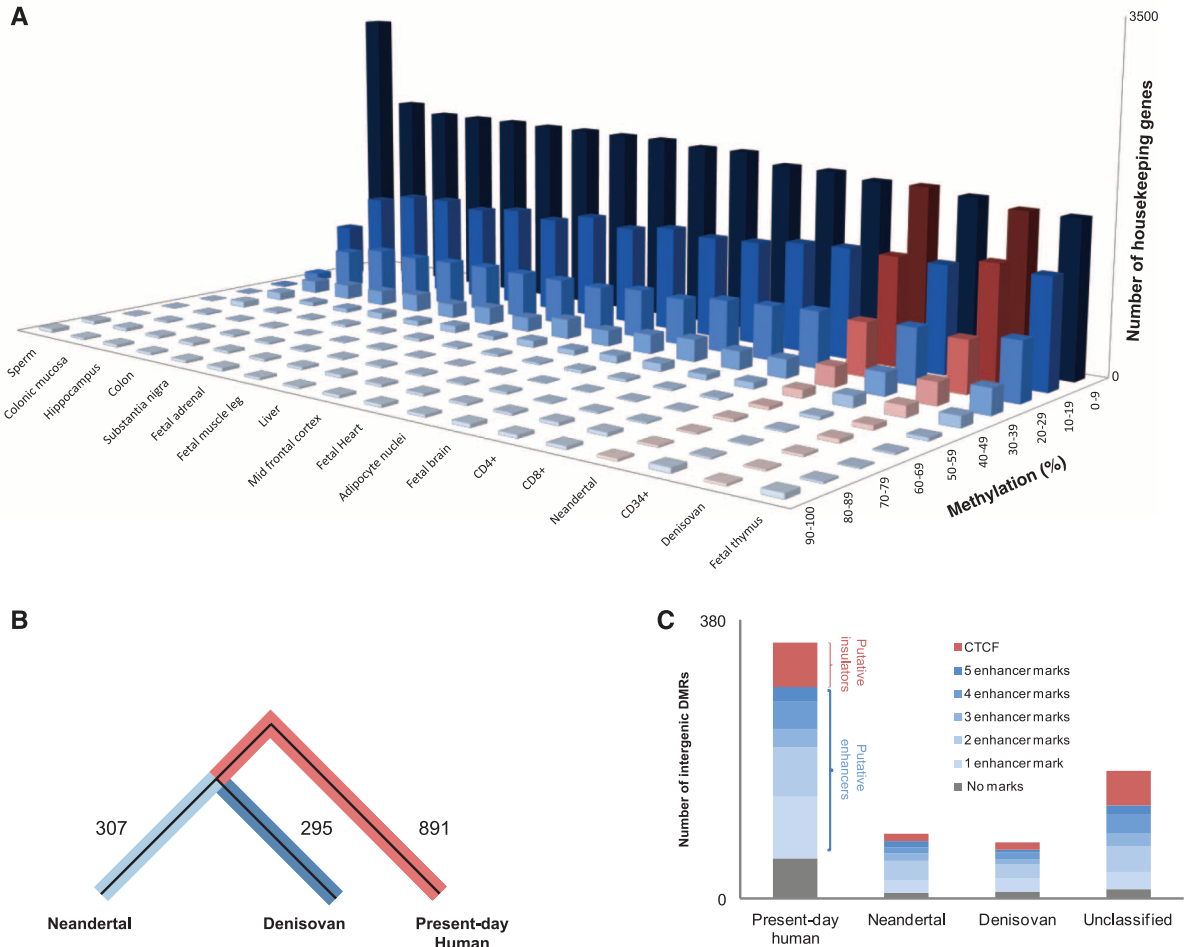


Fig. 3. Characteristics of DMRs. (A) Distribution of methylation in housekeeping promoters in various human tissues (blue) and in the Neandertal and the Denisovan (red). The distribution of methylation in the Neandertal and the Denisovan falls within the variability across human tissues. (B) The numbers of present-day human-, Neandertal-, and Denisovan-specific DMRs. (C) Inter-

genic DMRs colocalize with enhancer and insulator marks. Overlap of intergenic DMRs with insulator mark (CTCF) and with five different enhancer marks (histone modifications H3K4me1 and H3K27ac, histone variant H2A.Z, binding by p300, and DNase I sensitivity). DMRs are divided according to the number of enhancer marks they overlap.

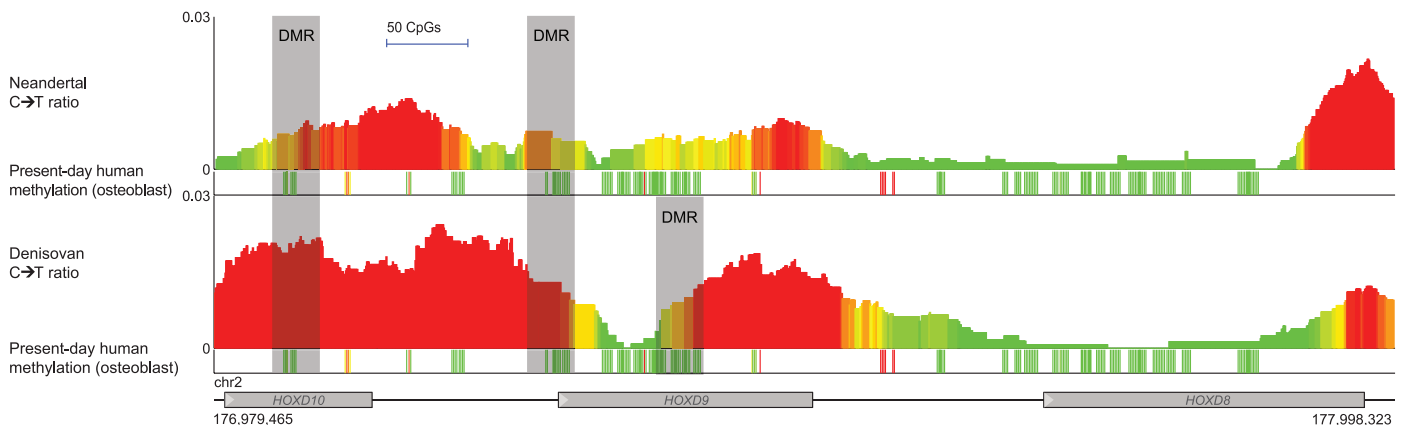


Fig. 4. The HOXD cluster is hypermethylated in archaic humans. C→T ratio in archaic humans, and present-day human methylation (see caption of Fig. 1C). Gray rectangles mark DMRs. A minimum of 10 positions with measured osteoblast methylation was required for a region to be denoted a DMR.

cluster in general and in *HOXD9* and *HOXD10* in particular (15, 21–23). Together, these findings suggest that the HOXD cluster might have played a key role in the recent evolution of human limbs.

Enhancers are often deoxyribonuclease I (DNase I)-sensitive regions bound by p300 and histone variant H2A.Z and marked by the histone modifications H3K4me1 and H3K27ac (24, 25). For insulators, CCCTC binding factor (CTCF) plays a major role as a buffer between active and inactive regions. By using a randomization test, we found a significant enrichment for enhancer marks and for CTCF binding in the intergenic DMRs, with over 80% having these marks (Fig. 3C, fig. S5, and tables S2 and S4). We show that this cannot be explained by length, CG-content, CpG density, or coverage (7). This suggests that many of the intergenic DMRs may affect gene activity through distal elements. Additionally, both of the intergenic DMRs upstream of the HOXD cluster possess enhancer marks (table S2), suggesting that they might have affected the methylation of the HOXD cluster through distal regulation.

DNA methylation affects, as well as is affected by, the binding of transcription factors (TFs) (3, 4). To test whether multiple DMRs may be associated with a change in a single TF, we looked for TF-encoding genes that are differentially methylated and whose targets are enriched with DMRs (7) (tables S5 and S6). In the Neanderthal, we identified sterol regulatory element binding protein 1 (SREBP-1), a regulator of lipid homeostasis ($FDR = 5.5 \times 10^{-3}$; Fisher's exact test), and aryl hydrocarbon receptor (AHR), a receptor of environmental toxins ($FDR = 3.7 \times 10^{-8}$). In present-day humans, we identified early growth response 3 (EGR3), which regulates biorhythm and development of muscles, lymphocytes, and neurons ($FDR = 4.2 \times 10^{-10}$); and Meis homeobox 1 (MEIS1), a regulator of limb development that forms complexes with both *HOXD9* and *HOXD10* ($FDR = 5.6 \times 10^{-8}$). This enrichment is independent of CpG density, GC content, and coverage (7). Additionally, the number of TFs that passed this test is significantly higher than would be expected by random ($P = 0.018$, hypergeometric test). These TFs could provide a lead to the mechanism behind the methylation changes and possibly offer a model of burstlike evolution, where multiple genes changed their activity after a single evolutionary event.

Last, we found that DMR-containing genes in present-day humans are almost twice as likely as genes that do not contain DMRs to be disease-related (18.1% compared with 10.8%, $P = 1.9 \times 10^{-7}$, Fisher's exact test) (fig. S6 and table S7). More than a third of the disease-linked genes (30/81) are involved in neurological and psychiatric disorders. Here, too, the enrichment is independent of gene length, CpG density, GC content, and coverage (7). This could potentially point to a link between recent changes in regulation and the emergence of diseases or to a scenario where disease-linked genes (i.e., genes in which a change

is not embryonic lethal) are possibly more prone to methylation changes.

Current techniques for measuring genome-wide methylation result in the destruction of the examined DNA (3) and are therefore impracticable in the study of ancient DNA. Our method allows for the reconstruction of methylation maps directly from ancient DNA reads without the need to use additional ancient material. We hope that the differences in methylation elucidated here will help to uncover the epigenetic basis for phenotypic differences between present-day and archaic humans and shed light on the role of epigenetics in the recent evolution of our lineage.

References and Notes

- M. Meyer *et al.*, *Science* **338**, 222–226 (2012).
- K. Prüfer *et al.*, *Nature* **505**, 43–49 (2014).
- P. A. Jones, *Nat. Rev. Genet.* **13**, 484–492 (2012).
- Z. D. Smith, A. Meissner, *Nat. Rev. Genet.* **14**, 204–220 (2013).
- A. W. Briggs *et al.*, *Nucleic Acids Res.* **38**, e87 (2010).
- J. S. Pedersen *et al.*, *Genome Res.* **24**, 454–466 (2014).
- Methods are available as supplementary materials on Science Online.
- ENCODE Project Consortium, *PLOS Biol.* **9**, e1001046 (2011).
- M. Rasmussen *et al.*, *Nature* **463**, 757–762 (2010).
- E. Eisenberg, E. Y. Levanon, *Trends Genet.* **29**, 569–574 (2013).
- M. J. Ziller *et al.*, *Nature* **500**, 477–481 (2013).
- J. E. Ohm *et al.*, *Cancer Res.* **70**, 7662–7673 (2010).
- S. H. Kresse *et al.*, *PLOS ONE* **7**, e48262 (2012).
- C. García-Ibarbia *et al.*, *Gene* **532**, 165–172 (2013).
- J. Zakany, D. Duboule, *Curr. Opin. Genet. Dev.* **17**, 359–366 (2007).
- P. Tschopp, D. Duboule, *Annu. Rev. Genet.* **45**, 145–166 (2011).
- F. M. Rijli, P. Dollé, V. Fraulob, M. LeMeur, P. Chambon, *Dev. Dyn.* **201**, 366–377 (1994).

- T. D. Weaver, *Proc. Natl. Acad. Sci. U.S.A.* **100**, 6926–6929 (2003).
- E. S. Mittra, H. F. Smith, P. Lemelin, W. L. Jungers, *Am. J. Phys. Anthropol.* **134**, 449–459 (2007).
- I. De Groot, *J. Hum. Evol.* **61**, 396–410 (2011).
- B. Dlugaszewska *et al.*, *J. Med. Genet.* **43**, 111–118 (2006).
- M. Fujimoto *et al.*, *J. Hum. Genet.* **43**, 32–36 (1998).
- C. C. de la Cruz, A. Der-Avakian, D. D. Spyropoulos, D. D. Tieu, E. M. Carpenter, *Dev. Biol.* **216**, 595–610 (1999).
- C. T. Ong, V. G. Corces, *Nat. Rev. Genet.* **12**, 283–293 (2011).
- M. Ku *et al.*, *Genome Biol.* **13**, R85 (2012).

Acknowledgments: We thank S. Shifman, Y. Stelzer, M. Choder, O. Amster-Choder, U. Ben-David, M. Meyer, Y. Aaronson, and Y. N. Harari for critical comments. Supported by the Israel Science Foundation FIRST individual grant (ISF 1430/13 to L.C. and E.M.), the Israel Science Foundation (ISF 1252/12, 657/12 to E.M.), a European Union Marie Curie Reintegration grant (IRG-248639 to L.C.), the Abisch-Frenkel Foundation (to E.M.), the European Research Council (ERC-281781 to E.M.), the Presidential Innovation Fund of the Max Planck Society (to S.P.), and the Spanish Health Ministry (Instituto de Salud Carlos III-FIS PI09/539, PI12/615). Software (RoAM, after Reconstruction of Archaic Methylation) can be found at <http://carmelab.huji.ac.il/software/RoAM/roam.html> and data at <http://carmelab.huji.ac.il/data.html>. The authors declare no competing financial interests. Requests for data should be addressed to Liran Carmel (liran.carmel@huji.ac.il) and Eran Meshorer (meshorer@huji.ac.il).

Supplementary Materials

www.sciencemag.org/content/344/6183/523/suppl/DC1
Materials and Methods
Figs. S1 to S6
Tables S1 to S10
References (26–43)

2 January 2014; accepted 4 April 2014
Published online 17 April 2014;
10.1126/science.1250368

Chemical Inhibition of NAT10 Corrects Defects of Laminopathic Cells

Delphine Larrieu,¹ Sébastien Britton,^{1*} Mukerrem Demir,¹
Raphaël Rodriguez,^{2†} Stephen P. Jackson^{1,3‡}

Down-regulation and mutations of the nuclear-architecture proteins lamin A and C cause misshapen nuclei and altered chromatin organization associated with cancer and laminopathies, including the premature-aging disease Hutchinson-Gilford progeria syndrome (HGPS). Here, we identified the small molecule “Remodelin” that improved nuclear architecture, chromatin organization, and fitness of both human lamin A/C-depleted cells and HGPS-derived patient cells and decreased markers of DNA damage in these cells. Using a combination of chemical, cellular, and genetic approaches, we identified the acetyl-transferase protein NAT10 as the target of Remodelin that mediated nuclear shape rescue in laminopathic cells via microtubule reorganization. These findings provide insights into how NAT10 affects nuclear architecture and suggest alternative strategies for treating laminopathies and aging.

Mutations in *LMNA*, which encodes lamin A and C, cause pathologies known as laminopathies (1), including the accelerated-aging disease Hutchinson-Gilford progeria syndrome (HGPS) (2, 3). Deregulation of A-type lamins expression or localization also

occurs in various cancers (4–6). Lamin A/C depletion or *LMNA* mutations cause enlarged, misshapen nuclei and altered chromatin organization (7). Whereas some of these pathologies might reflect cell fragility, many likely result from downstream effects on chromatin structure, gene